Journal of Power Sources 248 (2014) 273–282

Contents lists available at ScienceDirect

Journal of Power Sources

journal homepage: www.elsevier.com/locate/jpowsour

Formic acid electro-oxidation at PtAu alloyed nanoparticles synthesized by pulsed laser ablation in liquids

Daniel Nii Oko, Jianming Zhang, Sébastien Garbarino, Mohamed Chaker, Dongling Ma, Ana C. Tavares, Daniel Guay*

INRS-Énergie, Matériaux et Télécommunications, 1650 Boulevard Lionel-Boulet, Varennes J3X 1S2, Canada

HIGHLIGHTS

- PtAu alloy nanoparticles are formed by pulsed laser ablation in liquid.
- Catalysts made of a mixture of Pt and Au nanoparticles are studied.
- The structure of Pt and Au nanoparticles is modified through electrochemical aging.
- Electrochemically aged mixtures of Pt and Au nanoparticles behave like PtAu alloy NPs.

GRAPHICAL ABSTRACT

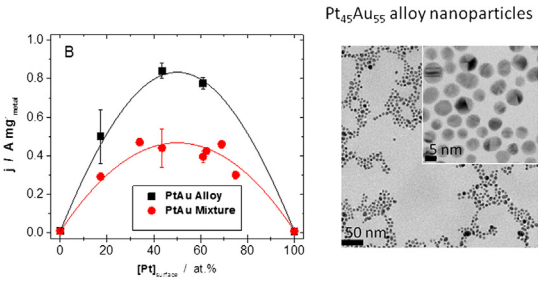

ARTICLE INFO

Article history:
Received 23 May 2013
Received in revised form
7 September 2013
Accepted 11 September 2013
Available online 25 September 2013

Keywords:
PtAu alloy
Laser ablation
Nanoparticle
Formic acid electro-oxidation
Catalyst

ABSTRACT

A series of mono dispersed Pt_xAu_{100-x} alloy nanoparticles (NPs), with x varying from 0 to 100, were prepared by pulsed laser ablation in liquids, using a series of targets that were made by mixing pure Pt and pure Au powders. The structures of Pt_xAu_{100-x} alloy NPs were assessed by transmission electron microscopy and X-ray diffraction. A face-centered solid solution is obtained over the whole composition range, and the particle size increases from 2.5 to 5.3 nm as x is increased from 0 to 100. The electrocatalytic performances of the Pt_xAu_{100-x} alloy NPs towards the formic acid oxidation were investigated by cyclic voltammetry and chronoamperometry. On as-prepared Pt_xAu_{100-x} alloy NPs, oxidation of formic acid occurs through dehydrogenation, while dehydration is the privileged mechanism on as-prepared mixtures of Pt and Au NPs. However, after a series of CV in 0.5 M H_2SO_4, both types of catalysts are able to oxidize formic acid according to the dehydrogenation pathway. After 600 s of electrolysis, the mass activities of Pt_xAu_{100-x} alloy NPs is a factor of two larger than that of mixtures of pure Pt and pure Au NPs with the same surface composition, although both types of catalysts display similar activity with respect to the total electrochemically active surface area.

1. Introduction

Direct formic acid fuel cells (DFAFCs) have a great potential as far as commercialization of fuel–cell system for portable electronic applications are concerned. This stems from the fact that formic acid is a non-toxic and high energy density fuel. Moreover, it is easily transported and stored [1]. Unlike methanol, formic acid has a lower permeability through Nafion®, allowing the use of concentrated formic acid, making DFAFCs a more promising option than direct methanol fuel cell (DMFC) [2]. In some cases, the performance of DFAFC approaches those of H_2-feed fuel cells [3].

Despite these numerous advantages, the commercialization of DFAFCs is hampered by the lack of cost effective and efficient catalysts for formic acid electro-oxidation [1]. Over the years, the use of Pt as electrocatalyst for formic acid electro-oxidation has been extensively studied [1]. However, Pt is not a suitable electrocatalyst

* Corresponding author.
E-mail address: guay@emt.inrs.ca (D. Guay).

0378-7753/$ – see front matter © 2013 Elsevier B.V. All rights reserved.
http://dx.doi.org/10.1016/j.jpowsour.2013.09.045

for this reaction because it is prone to poisoning by CO. This makes most of the Pt surface sites unavailable for further fuel oxidation, resulting in low overall current.

On Pt, the mechanisms responsible for the oxidation of formic acid include two reaction paths occurring in parallel [4]. The direct pathway (Eq. (1)) involves the dehydrogenation of formic acid molecule generating CO_2. In contrast, the indirect pathway (Eq. (2)) involves the dehydration of formic acid forming CO_{ads} that adsorbs strongly on the Pt surface.

$$HCOOH \rightarrow HCOO^-_{ad} + H^+ + e^- \rightarrow CO_2 + 2H^+ + 2e^- \quad (1)$$

$$HCOOH \rightarrow CO_{ad} + H_2O \rightarrow CO_2 + 2H^+ + 2e^- \quad (2)$$

Since high activity at low potentials is critical for high performance, the presence of CO_{ads} on the electrode surface is to be avoided and its effect diminished. This can be achieved on bimetallic surfaces with the second metal providing oxygen species at low potentials, thus facilitating the oxidative removal of CO_{ads} [5]. This effect is known as the bi-functional effect. Also, the presence of a second metal can cause a modification of the electronic structure of Pt and change the energy of adsorption of $CO_{ads,}$ leading possibly to a higher tendency of Pt to dehydrogenate formic acid molecule. This is known as the electronic effect. Another approach consists in facilitating the direct pathway by favoring the interruption of large Pt surfaces through the inclusion of foreign atoms. This effect is known as the third-body or the ensemble effect. It occurs because the indirect pathway needs at least three contiguous Pt atoms, whereas only two Pt atoms are needed for the direct pathway [6].

Using Density Functional Theory (DFT) calculations [7–9], it was recently pointed out there is a significant shift of the d-band center from −2.25 eV for Pt to −1.80 eV for PtAu alloys (and Pt overlayers onto Au). It is worth mentioning that the latter value is close to the d-band center of pure Pd (−1.83 eV), which is a well-known catalyst for the formic acid oxidation (FAO) through the dehydrogenation pathway [10,11]. Since then, Pt–Au bimetallic catalysts have been studied extensively and improved current efficiencies and lower tendencies to CO poisoning on these surfaces were demonstrated as compared to pure Pt [12–27]. While other metals like Pb [28] and Bi [29] showed similar promotion of the dehydrogenation path on Pt, the Pt–Au system is interesting because of the greater chemical stability of Au compared to these other elements. The enhanced electrochemical properties of PtAu bimetallic catalysts were attributed to the ensemble effect and to modification of the electronic structure of Pt atoms due to the presence of neighboring Au atoms.

Several strategies have been pursued to prepare PtAu bimetallic catalysts. In most studies, the PtAu bimetallic catalysts were prepared by reduction of Pt and Au salts using different reduction agents and solvents [12–15,17,18,22,23,30–37]. In some cases, the deposition of Pt and Au was achieved by first depositing a monolayer of Cu (UnderPotential Deposition (UPD) of Cu) and then proceeding to a Pt- or Au-redox replacement [16,21]. Other preparation methods of PtAu bimetallic catalyst include de-alloying of Pt–Cu–Au [19] or Al–Pt–Au [38,39], electrostatic self-assembly of positively charged Pt and negatively charged Au nanoparticles [20], electrodeposition of PtAu 3D foam films through hydrogen bubble dynamic templating [24], photoassisted reduction of Pt and Au salts [25], and galvanic replacement using sacrificial Ag templates of various forms [26]. Both unsupported [12,14,16,18–21,24,26,31] and supported [13,15,17,22,23,30,32] PtAu bimetallic catalysts were investigated. In most cases, high surface area carbon supports were used [13,15,17], although both graphene [22,23] and TiO_2 [25] were also used.

In the present paper, a systematic study of the influence of the composition and structure of PtAu bimetallic catalysts on the electrocatalytic activity for the FAO will be performed. Accordingly, Pt, Au, PtAu alloy nanoparticles (NPs) and mixture of Pt and Au NPs with controlled size and composition will be investigated. PtAu alloy NPs were prepared by pulsed laser deposition from a mixed Pt–Au single metal target with the appropriate composition [40], whilst mixtures of Pt and Au NPs were obtained by physically mixing Pt NPs and Au NPs. Through a detailed study of the NPs' electrochemical properties involving both cyclic voltammetry and chronoamperometry, a correlation is established between the surface composition of the PtAu alloy NPs and their electrocatalytic activity towards formic acid oxidation. Also, it will be shown that the surface structure and surface composition of physically mixed Pt and Au NPs can be modified through electrochemical aging, and that the activity and poisoning tolerance of the resulting materials approach that of PtAu alloy NPs, although the latter still exhibits larger mass specific electrocatalytic activity for the FAO.

2. Experimental section

2.1. Materials

Platinum (≥99.9%, 0.5–1.2 μm) and gold (≥99.9%, <10 μm) powders, sodium hydroxyl (NaOH) and hydrochloric acid (HCl) were purchased from Sigma–Aldrich and used without further purification. Nafion solution (5 wt %, Dupont), sulfuric acid (H_2SO_4, OmniTrace Ultra), and Amicon Ultra-4 Ultracel-50K centrifuge filters (Millipore) were obtained from Fisher Scientific. Water was deionized by a Millipore Ultrapure water system and has a resistivity of 18.2 MΩ cm at 25 °C.

2.2. Synthesis of PtAu colloids by pulsed laser ablation in liquid

For the preparation of PtAu alloy NPS, Pt and Au powders mixtures with different ratios (Pt_xAu_{100-x}, $x = 0$, 30, 50, 70, 100) were mechanically mixed for 30 min before being compression molded into a disk. In a typical process, 500 mg of Pt–Au powder mixture with the right composition was placed into a steel die with a diameter of 8 mm and pressed (CARVER Press, maximum pressure = 12 tons, during 10 min) to form a compact disk with a thickness of *ca* 1.5 mm. Then, this disk was used as a target to perform pulsed laser deposition in liquid [40]. All the operations were performed at room temperature.

The mixtures of Pt and Au NPs were prepared by physical mixing of pure Pt NPs and pure Au NPs that were obtained from pulsed laser deposition in liquid using pure Pt and pure Au targets, respectively. Mixtures of Pt_x and Au_{100-x} NPs were prepared by sampling the appropriate amount of Pt and Au NPs based solution using a micropipette. The mixtures were then sonicated for at least 20 min to form a uniform suspension which was drop-cast onto the surface of the supporting glassy carbon electrode. The dispersion of the nanoparticles on the glassy carbon electrode was evaluated from the diameter of the Pt, Au and $Pt_{50}Au_{50}$ nanoparticles determined by transmission electron microscopy and the electrochemically active surface areas (see below). In each case, the catalyst utilization, defined as the ratio between the surface areas calculated according to these two methods, was close to 100%, strongly suggesting that the nanoparticles are uniformly distributed at the surface of the glassy carbon support.

Neutron Activation Analysis (NAA) was used to assess the concentrations of the various elements. The analysis was performed on 1 mL of as-prepared colloidal solution using a SLOWPOKE nuclear reactor (Ecole Polytechnique de Montreal, Montreal, Canada).

2.3. Catalyst characterization

Transmission electron microscopy (TEM) samples were prepared by depositing a drop of colloidal solution onto a carbon-coated copper grid. The excess solution was wiped away with a filter paper. The grid was subsequently dried in air and examined using a JEOS-2100F TEM (École Polytechnique de Montréal). X-ray diffraction (XRD) analysis was performed by dropping highly concentrated colloidal solution on freshly cleaved single crystalline (311) silicon substrates. The sample was allowed to dry in air and the measurements were performed using a Panalytical XRD X-pert Pro diffractometer (Cu K_α, average wavelength = 1.5418 Å) to identify the phases present in the bimetallic catalysts The measurements were performed by fixing the incidence angle at 5°. The step size was 0.1° and the counting time was 15 s per step.

2.4. Electrochemical measurement

All electrochemical measurements were performed in a conventional three electrode electrochemical cell using a glassy carbon (GC) disk electrode (5 mm diameter, PineChem Inc) as the working electrode, a platinum gauze as the counter electrode and a saturated mercury/mercury sulfate electrode (Hg/Hg_2SO_4) as the reference electrode. Electrochemical potentials were finally converted and reported hereafter *versus* the reversible hydrogen electrode (RHE).

An adequate volume of the Pt_xAu_{100-x} colloidal suspension, corresponding in all cases to metal loadings of *ca.* 10 ± 0.3 $\mu g_{catalyst}$ cm^{-2}, was deposited onto the GC disk. After evaporation of the solvent, 3 μl of Nafion solution (5 wt.%) was pipetted onto the electrode and allowed to dry overnight. It is worth mentioning that preceding every electrode preparation, the GC disk substrates were polished with alumina slurries (1.0 μm and 0.05 μm diameters) and ultrasonically cleaned in pure water for 5 min.

All electrochemical studies were performed with an AUTOLAB (Eco Chemie) carried out at room temperature. Electrolyte solutions of 0.5 M H_2SO_4 (OmniTrace Ultra, Fisher Scientific) and 0.5 M HCOOH prepared with de-ionized water were de-areated with high purity Nitrogen (N4.8) for at least 30 min prior to measurements. Besides, a light flow of nitrogen was continuously maintained over the solution during electrochemical analyses.

The electrocatalytic activity of the materials for the FAO was assessed through CV (0.05–1.20 V, 50 mV s^{-1}) in 0.5 M H_2SO_4 + 0.5 M HCOOH solution previously purged with N_2 for 30 min. In most cases, an electrochemical aging step was conducted prior to the measurements of the FAO. This was achieved by performing a fixed number of CVs in 0.5 M H_2SO_4 (0.05–1.80 V, 100 mV s^{-1}), unless otherwise stated. In some cases, electrochemical aging was performed in a slightly different manner but this will be detailed later on. For potentiostatic measurements, current density *vs* time (*I*–*t*) curves were measured at a fixed potential of 0.56 V for 600 s.

3. Results and discussion

3.1. XRD characterization of the nanocatalysts

An XRD analysis of the Pt_xAu_{100-x} alloy and Pt_x + Au_{100-x} mixture NPs was carried out and some representative XRD patterns are shown in Fig. 1. The part of the XRD patterns where the characteristic diffraction peak of the Si (311) substrate occurs (from $2\theta = 53°–60°$) is not shown. XRD patterns of pure Au and pure Pt NPs are shown in curves A and B, respectively, along with the typical XRD pattern of a bimetallic nominal $Pt_{50}Au_{50}$ alloy (curve C). The XRD pattern of pure Au NPs exhibits five diffraction peaks,

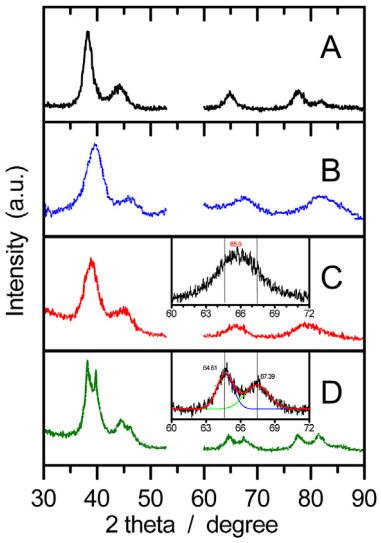

Fig. 1. X-ray diffraction patterns of (A) pure Au NPs, (B) pure Pt NPs, (C) nominal $Pt_{50}Au_{50}$ alloy NPs and (D) a nominal (50:50) mixture of pure Au NPs and pure Pt NPs.

corresponding to the {111}, {200}, {220}, {311} and {222} planes of a face-centered cubic (fcc) structure with a lattice parameter of 4.07 Å, while that of pure Pt NPs also exhibits the five characteristic diffraction peaks of a fcc structure with a lattice parameter of 3.92 Å. The XRD pattern of the nominal $Pt_{50}Au_{50}$ alloy NP catalysts displays also a single series of diffraction peaks corresponding to an fcc structure with a lattice parameter of *ca* 4.015 Å. It is noteworthy that no additional peaks (or set of peaks) are observed that would indicate that pure Au and pure Pt are present in this sample. The presence of a single set of diffraction peaks strongly indicates the formation of an alloy.

As mentioned in the experimental section, the nominal $Pt_{50}Au_{50}$ alloy NPs sample was prepared from the ablation of a target made of a physical mixture of Pt and Au powders. To further emphasize the fact that alloy NPs are formed in these conditions, the XRD pattern of a 50:50 nominal mixture of pure Pt NPs and pure Au NPs is shown as curve D of Fig. 1. As expected, two independent sets of diffraction peaks are observed in the XRD pattern. More interestingly, a high-resolution scan in a 2θ region centered at 65° clearly shows that the {220} peak of the nominal $Pt_{50}Au_{50}$ alloy is different from that of the 50:50 mixture of pure Au NPs and pure Pt NPs, emphasizing the fact that an alloy is formed between Pt and Au. Similar behavior was observed for Pt_xAu_{100-x} alloy NP catalysts prepared by varying the nominal Pt and Au content of the target although the position of the diffraction peaks vary with the value of *x* (data not shown). As detailed elsewhere [40], the variation of the lattice parameter with *x* follows Vegard's law as frequently observed in binary metallic alloys [35,41], confirming the formation of an alloy over a broad composition range. Based on a detailed analysis of XRD patterns, several authors have reached the same conclusion [14,19,24,26,31,34–36,39], emphasizing the fact a PtAu alloy can be formed in the appropriate conditions. As discussed elsewhere [42], this could arise because the heat of formation of alloy NPs exhibits notable size-dependence and that a negative heat of formation is obtained over the whole compositional range for PtAu alloy NPs not exceeding about 6 nm in diameter. As we will see later on, this condition is fulfilled in this work.

Using the Scherer's equation and the full width at half maximum (FWHM) of the diffraction peaks, it was estimated that the crystallite size of the NPs increases from ~2.7 to ~5.2 nm as the amount of Au in the target increases from 0 to 100 at.%.

3.2. TEM imaging of the nanoparticles

The Pt_xAu_{100-x} alloy NPs samples were characterized using TEM. Representative micrographs of Pt, Au and nominal $Pt_{50}Au_{50}$ alloy NPs samples are shown in Fig. 2. The micrograph of Pt (Fig. 2A) shows a collection of well dispersed metal NPs with an average diameter of 2.5 ± 1.1 nm. The particle size was determined by measuring more than 100 individually dispersed particles. The micrograph of Au NPs (Fig. 2B) shows well-dispersed NPs of approximately spherical shape. The average particle size is 5.2 ± 1.6 nm. Fig. 2C presents an image of nominal $Pt_{50}Au_{50}$ alloy NPs with many individually dispersed particles, along with partially coalesced particles and some irregularly shaped nanostructures, such as nanorods. The average size, based on the measurement of 100 dispersed particles, is 3.9 ± 1.7 nm. Nominal $Pt_{70}Au_{30}$ and $Pt_{30}Au_{70}$ alloy NPs were also prepared and analyzed by TEM (not shown here). These samples behave similarly to $Pt_{50}Au_{50}$ alloy NPs with an average particle diameter of 2.8 ± 0.8 nm and 3.4 ± 1.6 nm for $Pt_{70}Au_{30}$ and for $Pt_{30}Au_{70}$, respectively. These values are close to those determined from XRD analysis, indicating that these NPs are basically single crystals.

3.3. Electro-oxidation of formic acid

To evaluate the electrocatalytic activity towards FAO, the whole range of Pt_xAu_{100-x} alloy and $Pt_x + Au_{100-x}$ mixture NPs catalysts were investigated by cyclic voltammetry (CV), and some representative results for $Pt_{50}Au_{50}$ alloy NPs and $Pt_{70} + Au_{30}$ nominal mixture of NPs are displayed in Fig. 3. The curves displayed in Fig. 3 are the 20th cycle performed in 0.5 M H_2SO_4 and 0.5 M HCOOH solution (between 0.0 and 1.2 V). The shape of the CVs remained the same from the first to the 20th cycle, with the maximum current varying by less than 20%.

It was found that electrochemical aging is critical in influencing the electrocatalytic activity of $Pt_x + Au_{100-x}$ mixture NPs. Accordingly, CV profiles of freshly prepared $Pt_{70} + Au_{30}$ mixture NPs (nominal composition) in formic acid solution are shown in Fig. 3A, and after electrochemical aging in Fig. 3B–D. The aging consisted in potential cycling between 0.05 and 1.80 V (at 100 mV s^{-1}) in 0.5 M H_2SO_4 for 2 cycles (Fig. 3B), 10 cycles (Fig. 3C) and 50 cycles (Fig. 3D) in sulfuric acid solution prior to the CV in formic acid are displayed. For comparison, the CVs in 0.5 M H_2SO_4 + 0.5 M HCOOH of electrochemically aged (50 cycles, between 0.05 and 1.80 V at 100 mV s^{-1}) pure Pt NPs (Fig. S1A) and pure Au NPs (Fig. S1B) are shown in the Supporting information section.

For electrochemically aged Pt NPs, two different anodic contributions are observed in the forward scan with a first current peak (peak 1) located at *ca* 600 ± 20 mV, which is related to the direct oxidation of HCOOH to CO_2 via a dehydrogenation pathway. The second peak (peak 2) occurs at *ca* 920 ± 20 mV, and is associated with the oxidation of a CO-type surface intermediates (quoted as CO_{ads}) that are concomitantly generated with the oxidation of formic acid via the dehydration pathway. For pure Au NPs, a single oxidation current contribution is observed at *ca* 520 mV (peak 1). However, this peak current is quite low, confirming the poor electrocatalytic activity of Au NPs for FAO [15].

It is well known from the literature that the ratio between the maximum current reached at peak 1 and peak 2 can be used to

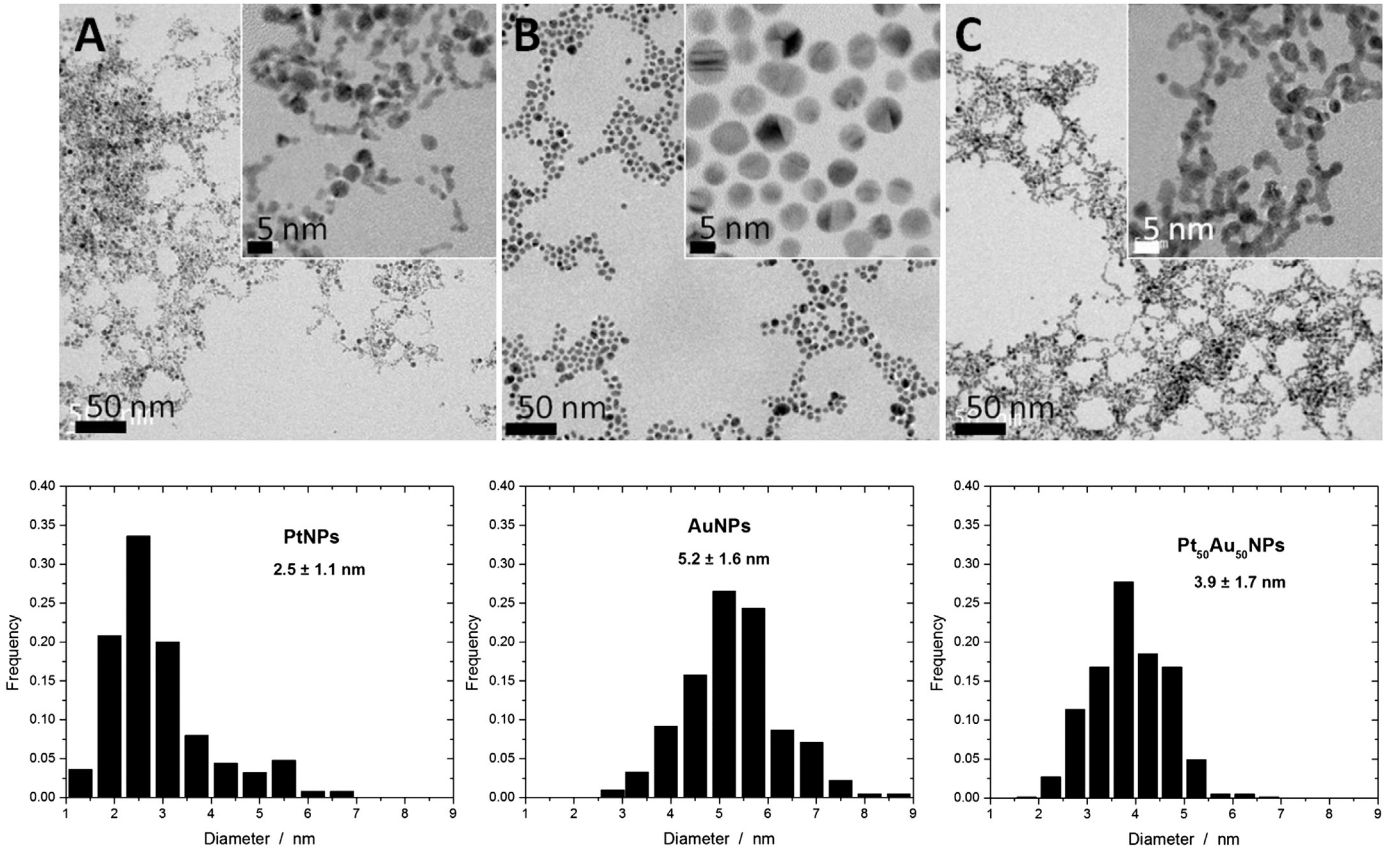

Fig. 2. Transmission electron microscopy micrographs of (A) Pt, (B) Au and (C) nominal $Pt_{50}Au_{50}$ alloy NPs. The insert to each micrograph shows a higher magnification of the same sample. The size distribution is shown below each micrograph.

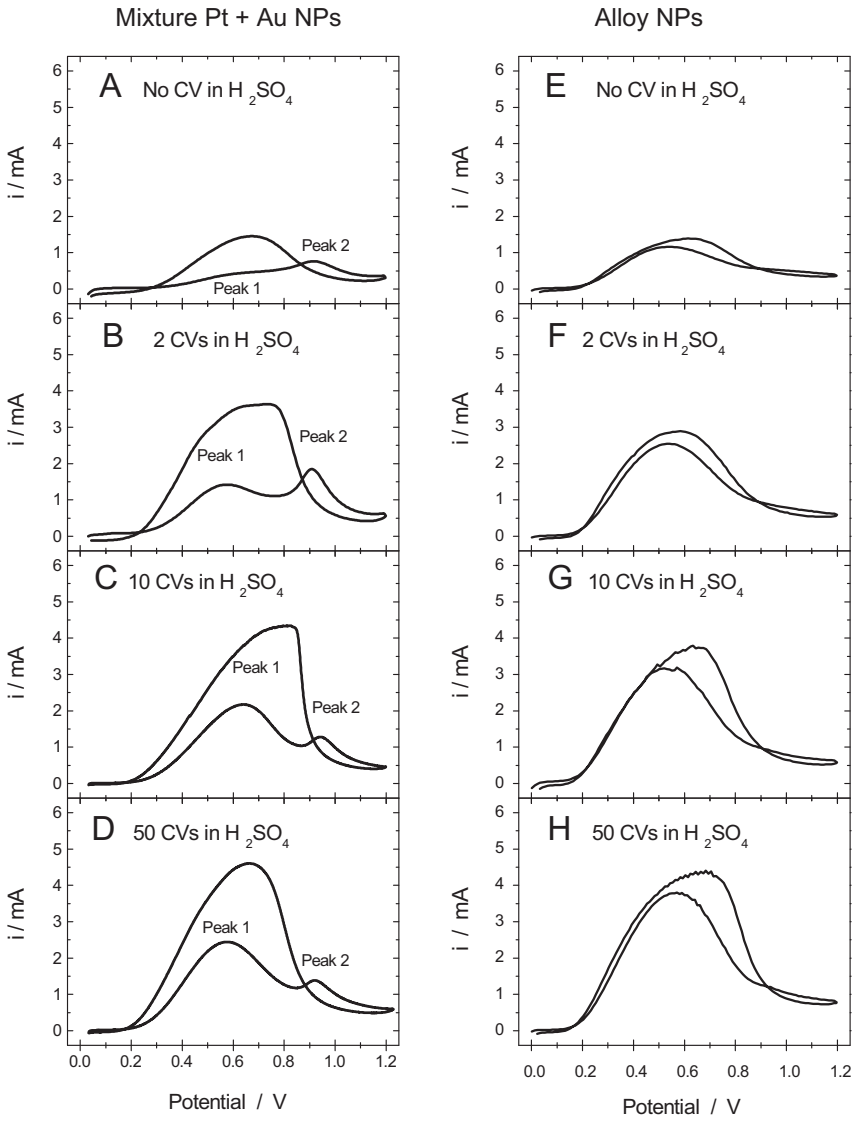

Fig. 3. Stable CVs (50 mV s^{-1}) of (A–D) a nominal (70:30) mixture of Pt and Au NPs, and (E to H) a nominal $Pt_{50}Au_{50}$ alloy NPs in 0.5 M H_2SO_4 + 0.5 M HCOOH. An electrochemical aging process was previously applied which consists in cycling the material in 0.5 M H_2SO_4 between 0.05 and 1.80 V for a fixed number of cycles (A and E) 0 cycle, (B and F) 2 cycles, (C and G) 10 cycles, and (D and H) 50 cycles.

assess the degree of tolerance with respect to CO_{ads} formation and the relative importance of the dehydrogenation and dehydration pathways. On Pt NPs, the peak current density of peak 2 (i_{p2}) is higher than that of peak 1(i_{p1}) and the ratio i_{p1}/i_{p2} is *ca* 0.33. This is similar to the i_{p1}/i_{p2} value (*ca* 0.2–0.7) found elsewhere for Pt black and various other forms of pure Pt catalysts [15,26]. This is clear indication that the FAO occurs mainly through the indirect pathway on Pt NPs, independently of the preparation procedure.

As seen in Fig. 3A, the shape of the CV and the i_{p1}/i_{p2} value of as-prepared Pt_{70} + Au_{30} mixture NPs catalysts are similar to that of pure Pt NPs, suggesting that the dehydration pathway is dominant. This is not surprising considering that this sample is made by physically mixing both Pt and Au NPs. However, following electrochemical aging, the value of i_{p1} (i_{p2}) increases (decreases) steadily, resulting in a steady increase of the ratio i_{p1}/i_{p2} with the number of potential cycles in H_2SO_4. For example, the ratio i_{p1}/i_{p2} is 0.8 after 2 CVs in H_2SO_4 and 1.7 after 10 CVs. This effect levels off and the ratio i_{p1}/i_{p2} does not increase significantly if the electrochemical aging process is prolonged up to 50 cycles, in which case the ratio i_{p1}/i_{p2} reaches 1.9. Clearly, the surface of the catalysts made of a physical mixture of Pt and Au NPs is altered and this modification favors the dehydrogenation pathway.

As noted in Fig. 3A–D, this modification of mechanisms is also accompanied by an increase of the electrocatalytic activity of the materials for the FAO, as evidenced by the gradual increase of the maximum current reached on the reverse scan. Indeed, the maximum current on the reverse scan increases from 1.5 to 4.6 mA as a result of the electrochemical aging process. A similar phenomenon was observed for all the Pt_x + Au_{100-x} mixture NPs catalysts. These results suggest that potential cycling in sulfuric acid prior to FAO is crucial to increase the electrocatalytic activity towards the FAO and to alter the reaction mechanisms governing the FAO.

The CV profile in formic acid of as-prepared $Pt_{50}Au_{50}$ alloy NPs and after electrochemical aging (2, 10 and 50 cycles) are displayed Fig. 3E–H, respectively. It is observed that:

(i) The CV of as-prepared $Pt_{50}Au_{50}$ alloy NPs is strikingly different from that of as-prepared Pt_{70} + Au_{30} mixture NPs catalysts. Indeed, on the forward scan, the current of peak 1 is

higher than the current of peak 2, resulting in a i_{p1}/i_{p2} ratio of 2.2, several times larger than that found for the mixture of Pt and Au NPs. This is strong evidence that the FAO proceeds mainly through the dehydrogenation mechanism at the surface of as-prepared $Pt_{50}Au_{50}$ alloy NPs, unlike what was observed previously on as-prepared mixtures of Pt and Au NPs. This conclusion is reinforced by the fact that the forward and the backward scans are almost superimposed on each other, indicating that oxidation of the catalyst at the upper potential limit of the scan does not cause any drastic change, essentially because the amount of CO_{ads} is minimal. This is in clear contrast with the as-prepared $Pt_{70} + Au_{30}$ mixture NPs catalysts, where a large hysteresis is observed between the forward and backward scans. In that case, this is indicative that removal of CO_{ads} at the upper potential limit freed the surface from its contaminants.

(ii) There is no change in the shape of the CVs with electrochemical aging. Indeed, the current associated with peak 1 is always larger than that of peak 2. After 50 cycles in H_2SO_4, the i_{p1}/i_{p2} ratio for $Pt_{50}Au_{50}$ alloy NPs is 3.78. The value is in close agreement with the ip_1/ip_2 ratio value of 3.57 independently reported elsewhere for PtAu alloy NPs [12]. This indicates that the FAO occurs through the more desirable dehydrogenation pathway on PtAu alloy NPs, whether or not the catalyst has been electrochemically aged. This is radically different from the previous case (mixture of Pt and Au NPs), where it was observed that the shape of the CV evolves dramatically with electrochemical aging.

(iii) The current maximum of the CVs increases steadily from *ca* to 1.3–4.3 mA with electrochemical aging.

It is interesting to note that the CV profiles of electrochemically aged mixture of Pt and Au NPs (Fig. 3D) and PtAu alloy NPs (Fig. 3H) are quite similar (although not identical). For example, in Fig. 3H, the current contribution at 920 mV (dehydration path) is hardly discernible, whereas that current contribution is still present for the electrochemically aged mixtures of Pt and Au NPs (Fig. 3D). The absence of this feature in the case of the PtAu alloy NPs suggests a more homogenous surface repartition of the Pt–Au ensemble catalytic sites, giving rise to a single current peak at 560 mV that indicates that the FAO occurs almost exclusively through the dehydrogenation pathway. It is clear that electrochemical aging of mixtures of Pt + Au NPs drastically changed the composition and structure of the catalyst surface but the presence of a non-negligible current at 920 mV (peak 2) in the CV profile of electrochemically aged mixture of Pt and Au NPs indicates that some Pt-like surface domains remained present and that the FAO still proceeds to a certain extent via the partial dehydration pathway.

A series of additional experiments were realized to get further insights on the effect of electrochemical aging on the surface properties of the Pt + Au mixture NPs and on their activity towards FAO. First, a similar series of measurements were realized by decreasing the upper potential limit of the CV during the electrochemical aging procedure. Thus, two freshly prepared (70:30) mixtures of Pt and Au NPs were subjected to potential cycling (50 cycles in 0.5 M H_2SO_4) between 0.05 V and 1.50 V, and between 0.05 V and 1.20 V. In the first case (1.5 V upper potential), the CV of the resulting material recorded in 0.5 M H_2SO_4 + 0.5 M HCOOH (see Fig. S2) is similar to the one obtained previously for an upper potential of 1.80 V (Fig. 3D). This is in striking contrast to what happen when the upper potential is reduced to 1.20 V. In that later case, the shape of the CV of the resulting material recorded in 0.5 M H_2SO_4 + 0.5 M HCOOH (see Fig. S3) does not evolve with the number of cycles (up to 50 cycles were performed), indicating that the FAO occurs mainly through the indirect pathway as on pure Pt NPs.

Finally, the effect of conducting the electrochemical aging process by holding the potential at a constant value (instead of cycling it between a lower and an upper limit) was investigated. Thus, two freshly prepared (70:30) mixtures of Pt and Au NPs were polarized at 1.50 and 1.80 V in 0.5 M H_2SO_4 during 30 min before being transferred to a HCOOH + H_2SO_4 solution where CVs were recorded. As seen in Fig. S4A and B for 1.50 and 1.80 V, respectively, the shape of the CVs resemble closely to those recorded for Pt (see Fig. 3A), with an i_{p1}/i_{p2} value of *ca* 0.5. These potential limits are the same as those used previously in Fig. S2 and Fig. 3. Obviously, holding the electrode potential at the upper potential limit is not enough to change the mechanisms responsible for the FAO on the Pt + Au mixture NPs. The reasons for this will become clear in the next section.

3.4. Surface properties of the nanocatalysts

Cyclic voltammetry (CV) is a surface sensitive technique used to assess the electrochemical properties of surface atoms (rather than bulk atoms). Elsewhere, CV was used to study the influence of potential cycling on the electrochemically active surface area (EASA) and on the surface composition of PtAu bimetallic catalysts [15,19,24,40]. The EASA and the surface composition of the samples at their different states of electrochemical aging were assessed through a detailed analysis of the CVs recorded in 0.5 M H_2SO_4.

CVs in 0.5 M H_2SO_4 of a nominal (70:30) mixture of Pt + Au NPs and nominal $Pt_{50}Au_{50}$ alloy NPs are depicted in Fig. S5A and C, respectively. In that case, the upper potential was set to 1.8 V. On gold, monolayer oxide formation starts at 1.35 V during the forward sweep, and the gold oxide reduction peak in the backward potential sweep occurred at *ca* 1.13 V. Therefore, the reduction peak observed at *ca* 1.10 V is attributed to the presence of gold atoms at the surface of the materials. The electrochemically active surface area of gold (Au EASA) was determined by integrating the charge associated with the Au oxide reduction peak and by using a factor of 400 μC cm^{-2} for the reduction of Au α-oxide film grown up to 1.8 V in sulfuric acid [43].

In Fig. S5A and C, the typical features of polycrystalline Pt surfaces are distinguishable. On these CVs, Pt oxide film formation occurred at *ca*. 0.85 V and oxide reduction occurs at *ca* 0.70 V on the reverse scan. In the low potential region, a pair of hydrogen adsorption/desorption peaks are observed at 0.13 V and 0.27 V, typical polycrystalline Pt surfaces. In most studies, the hydrogen adsorption/desorption region is used to assess the Pt EASA. However, in cases where Pt is alloyed with a different metal atom, it was shown elsewhere that this leads to an underestimation of the true EASA [44]. Therefore, to alleviate any concerns, the current associated with the Pt oxide reduction peak was used to calculate the Pt EASAs. However, when the upper potential is 1.8 V like it is in Fig. S5A and C, a precise evaluation of the Pt surface content cannot be obtained since more than a monolayer of platinum oxide is grown on the platinum surface, concomitantly with oxygen gas evolution [43,45]. Therefore, to evaluate the electrochemically active surface area of platinum (Pt EASA), the upper potential limit of the CV was lowered to 1.5 V, which is the potential at which a monolayer of surface Pt oxide is formed [46,47], assuming a factor of 440 μC cm^{-2} of surface Pt atoms [46]. CVs used to evaluate the Pt EASA are shown as representative examples in Fig. S5B and D for a nominal (70:30) mixture of Pt + Au NPs and $Pt_{50}Au_{50}$ alloy NPs, respectively.

The evolution of the Pt and Au EASAs with electrochemical aging is depicted in Fig. 4A and C for a nominal (70:30) mixture of Pt + Au NPs and $Pt_{50}Au_{50}$ alloy NPs, respectively. As seen in Fig. 4A, both Pt and Au EASAs decreased with potential cycling from 1.32 to 0.56 cm^2_{Pt} and from 0.76 to 0.55 cm^2_{Au}, respectively. In comparison,

the Pt and Au EASAs decrease from 1.12 to 0.51 cm^2_{Pt} and from 1.21 to 0.71 cm^2_{Au}, respectively, in the case of the nominal $Pt_{50}Au_{50}$ alloy NPs. This decrease is more drastic at the beginning of the aging process and levels off with the number of cycles.

In Fig. 4A and C, the decrease of the Pt and Au EASAs is similar to that observed when pure Pt NPs and pure Au NPs are cycled in the same conditions. For example, Pt NPs cycled in 0.5 M H_2SO_4 up to 1.5 and 1.8 V exhibits a steady decrease of current associated with the various features of the CV and a concomitant decrease of the Pt EASA (see Fig. S6A and B, respectively, for a representative example with a potential limit of 1.5 V). In contrast, there is almost no change in the CVs if the upper potential is reduced to 1.2 V (see Fig. S6C), indicating there is no change of the EASA with potential cycling. In the case of pure Au NPs, the same observations can be made except that a more positive potential limit is required to observe a significant change of the Au EASA. As shown in Fig. S6D and E, there is an appreciable decrease of the Au EASA for a potential limit of 1.8 V, while CVs remain unchanged when the potential limit is 1.5 V (see Fig. S6F).

The EASA loss for Pt [48] and Au [49,50] NPs under potential cycling conditions was extensively studied in previous reports. The suggested mechanisms include interface processes such as sintering, dissolution, coalescence and Ostwald ripening. However, the mechanisms responsible for the decrease of the EASA cannot be unequivocally identified from curves like those shown in Fig. 4 since all of them leads to a diminution of the EASA. It is beyond the scope of this study to give a detailed account of the mechanisms responsible for the decrease of the EASA. Nevertheless, it is important to emphasize that Pt atoms re-organization, which is indicated by a decrease of the Pt EASA, occurs only for potential cycling up to 1.5 and 1.8 V, which are the upper potential of the electrochemical aging process at which the Pt-like behavior disappears and the alloy-like behavior appears during the FAO on mixtures of Pt and Au NPs (see Fig. 3, Figs. S2 and S3).

The value of the upper potential during the CV performed in 0.5 M H_2SO_4 is not the sole determining factor for the development of the alloy-like behavior during FAO on mixtures of pure Pt and pure Au NPs. Indeed, as shown in Fig. S4, holding the electrode potential at 1.5 or 1.8 V for an extended period of time (30 min) does not lead to the appearance of the alloy-like behavior. This observation emphasizes the fact that the excursion of the potential to value lower than 1.5 and 1.8 V (potential cycling) is critical to achieve the atomic surface re-arrangement responsible for the change in the mechanisms responsible for the FAO in the mixture of Pt + Au NPs.

All these observations can be reconciled if one considers that Pt and/or Au dissolution and re-deposition could occur during potential cycling if the value of the upper potential is sufficiently large. This hypothesis is consistent with a recent study by Mayrhofer et al. [51] that measured the dissolution rates (ng cm^{-2} $cycle^{-1}$) of extended surfaces of Au and Pt with potential cycling in sulfuric acid solution. Thence, for cycling up to 1.50 V and 1.80 V (RHE), the dissolution rates of Pt are 5.8 and 9.0 ng cm^{-2} $cycle^{-1}$, respectively, while that of Au are 4.4 and 20.0 ng cm^{-2} $cycle^{-1}$, respectively. In the present case, the dissolution rates of both Pt and Au nanoparticles might even be higher than these values since the dissolution rate of metal nanoparticles increases as the particle size decreases due to the larger specific surface energy [52]. The hypothesis is also consistent with the fact that electrochemical deposition of platinum and gold occurs readily at potential as large

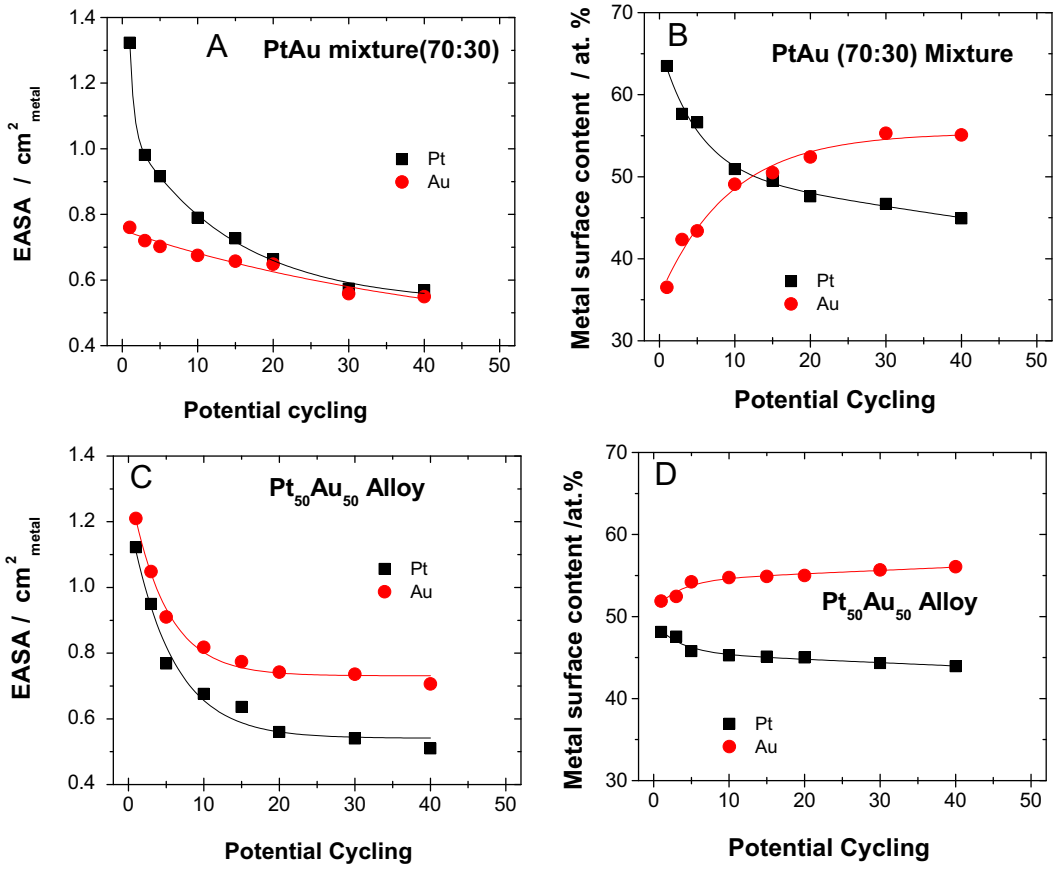

Fig. 4. Effect of potential cycling on (A and C) the electrochemically active surface area (EASA) and (B and D) the surface composition of (A and B) a nominal (70:30) mixture of Pt and Au NPs, and (B and D) nominal $Pt_{50}Au_{50}$ alloy NPs. The potential cycling was performed in 0.5 M H_2SO_4 and between 0.05 and 1.80 V for a fixed number of cycles.

as 0.7 V (NHE) [53,54] and 1.0 V (NHE) [55], respectively, well above the lower potential of the CV performed during the electrochemical aging process. Electrochemical Quartz Crystal Microgravimetry studies already mentioned dissolution and redeposition of both Au [56] and Pt [53] during cyclic voltammetry experiments in sulfuric acid solution. It is worth mentioning that this behavior was only observed if the upper potential limit of the CV was set up in the oxide potential region.

Thus, it is hypothesized that the change in the mechanisms responsible for the FAO on the mixtures of Pt + Au NPs occurs as a result of the dissolution and re-deposition of both Pt and Au atoms during the electrochemical aging process if the upper potential is 1.5 and 1.8 V. During this process, re-deposition must occur in such a way that Pt and Au atoms become intimately mixed. The exact structure (Pt deposited on gold NPs, Au deposited on Pt NPs, co-deposition of Pt and Au to form an alloyed NP) of the catalysts at the end of the electrochemical aging process is difficult to assess from the present results. However, data from the literature have shown that suppression of the formation of poisoning intermediate CO is observed in the following cases: (i) deposition of Pt on Au nanorods and nanoparticles [15,16], (ii) deposition of Au on a Pt surface [21], and electrodeposition from a solution containing a mixture of Pt and Au salts [24]. Moreover, as recently pointed out, the surface of the Pt-on-Au system is not frozen and potential-dependent surface exchange occurs between Pt and Au atoms, allowing both atoms to migrate onto the surface [57]. Considering the similitude between the experimental conditions of that study and those of the present study, this aging process might contribute to the development of a catalyst surface composed of an intimate mixture of Pt and Au atoms. Indeed, it was shown elsewhere that the presence of both Pt and Au atoms at the surface of the catalysts are needed to favor the dehydrogenation over the dehydration pathway [15,58]. These two studies showed that FAO proceeds mostly through the dehydrogenation pathway when the coverage of Pt on the Au substrate is low, but then changes to the dehydration pathway as the Pt coverage is increased beyond a monolayer and gold atoms are not accessible to the electrolyte.

As it can be qualitatively assessed from a visual inspection of the curves shown in Fig. 4A and C, the rate of decrease of the Pt and Au EASAs varies from one type of catalyst to the other, causing a change in the surface composition of the catalysts with respect to the nominal surface composition. Therefore, to assess the effect of the electrochemical aging process on the surface composition of the materials, the Pt surface content ($[Pt]_{surface}$) of the Pt_xAu_{100-x} mixture and Pt_xAu_{100-x} alloy NPs was evaluated through the following equation

$$[Pt]_{surface} = EASA_{Pt}/(EASA_{Pt} + EASA_{Au}) \quad (3)$$

where $EASA_{Pt}$ and $EASA_{Au}$ are the electrochemically active surface areas (cm^2) of platinum and gold, respectively. As seen in Fig. 4B and D, the Pt surface content of the (70:30) nominal mixture of Pt + Au NPs decreases from 65 to 44 at.% upon potential cycling, while the Au surface increases from 35 to 56 at.%. Thus, the surface composition of the physically mixed Pt + Au NPs samples is drastically changed by the electrochemical aging process. In comparison, the surface composition of the PtAu alloy NPs is hardly modified during the same electrochemical aging process and the Pt surface content decreases from 48 to 45 at.%, while the Au surface content increases from 52 to 55 at.%. The final surface composition on the nominal $Pt_{50}Au_{50}$ alloy electrode remains very close to the composition of the as-prepared catalyst, even if there is a significant decrease of the Pt and Au EASAs.

Fig. 5 summarizes the evolution of the Pt surface content *versus* the nominal Pt content of Pt_xAu_{100-x} alloys and $Pt_x + Au_{100-x}$ mixtures NPs after electrochemical aging (upper potential of 1.8 V) in 0.5 M H_2SO_4. The CVs that were used to assess the final surface composition of $Pt_{30}Au_{70}$ and $Pt_{70}Au_{30}$ alloy NPs, and nominal (30:70) and (50:50) Pt + Au NPs mixtures are shown in Figs. S7and S8, respectively. In all cases, there is a depletion of Pt atoms at the surface of the catalysts compared to the nominal Pt content. This effect is more pronounced on the mixtures of Pt and Au NPs. In the following, the different catalyst materials will be designated by their actual surface composition.

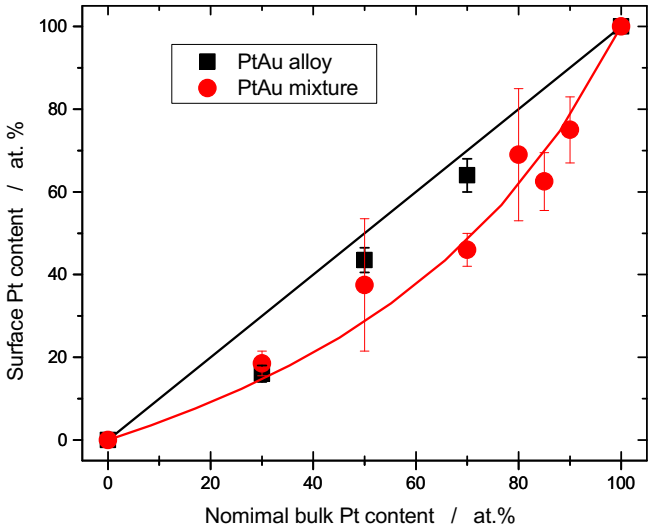

Fig. 5. Variation of the Pt surface content as a function of the Pt bulk content following electrochemical aging of catalysts that consists in potential cycling between 0.05 and 1.80 V in 0.5 M H_2SO_4 (50 mV s^{-1}).

3.5. Steady-state activity towards formic acid oxidation

The chronoamperometric technique was used to further probe the steady-state activity of the $Pt_x + Au_{100-x}$ mixtures and Pt_xAu_{100-x} alloys NPs after electrochemical aging in H_2SO_4 (50 cycles, potential limit of 1.8 V). As representative examples, the chronoamperometric curves of pure Pt NPs, $Pt_{45}Au_{55}$ alloy NPs, $Pt_{44} + Au_{56}$ mixture NPs and pure Au NPs electrodes in 0.5 M H_2SO_4 + 0.5 M HCOOH are displayed in Fig. 6A–D, respectively. This series of measurements were realized by first holding the electrode potential at 0.25 V (10 s) and then stepping it up to 0.56 V (600 s). At the end of the electrolysis period ($t = 600$ s), low current values (*ca* 0.01 A mg^{-1}_{metal}) are observed for pure Au NPs and pure Pt NPs, reflecting the fact that these materials exhibit a poor intrinsic activity and a fast poisoning, respectively. In comparison, the current density after 600 s on the $Pt_{45}Au_{55}$ alloy NPs is 0.84 A mg^{-1}_{metal}, a factor of 80 larger than on pure Pt NPs, and *ca* 0.44 A mg^{-1}_{metal} on the electrochemically aged mixture of $Pt_{44} + Au_{56}$ NPs. This improvement over the performance of pure Pt NPs clearly indicates that the introduction of Au atoms endows the catalyst with a much higher steady-state current density. A similar improvement of the electrocatalytic activity for the FAO resulting from the mixing of Pt and Au atoms was already demonstrated elsewhere. For example, graphene-supported bimetallic $Pt_{50}Au_{50}$ nanoparticles have been shown to exhibit a much higher current density than pure graphene-supported Pt nanoparticles [23,24].

The value of the steady-state current density recorded after 600 s of polarization is plotted in Fig. 7 with respect to the actual surface composition of the materials. In that figure, the current

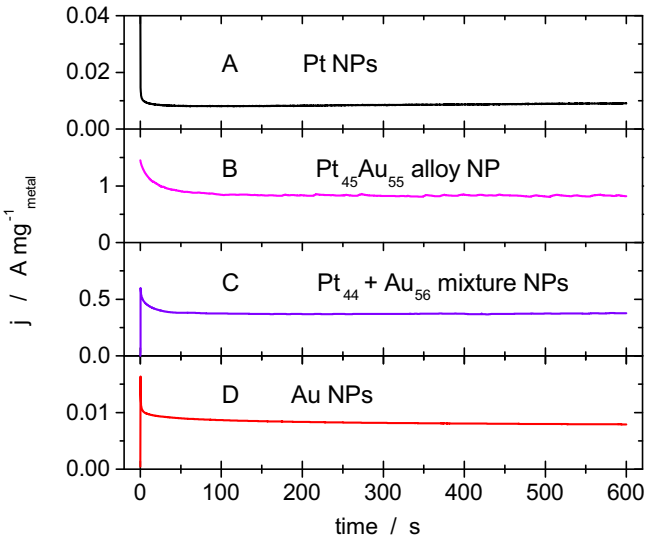

Fig. 6. Chronoamperometric curves (E_{appl} = 0.56 V in 0.5 M H_2SO_4 + 0.5 M HCOOH) of electrochemically aged (A) pure Pt NPs, (B) $Pt_{45}Au_{55}$ alloy NPs, (C) Pt_{44} + Au_{56} mixtures of Pt and Au NPs, and (D) pure Au NPs. The actual composition of materials was used for their identification.

densities are expressed with respect to the experimentally determined total EASA (Pt + Au) (mA $cm^{-2}{}_{metal}$, see Fig. 7A), and with respect to the total initial mass of metal deposited on the electrode (mA $mg^{-1}{}_{metal}$ see Fig. 7B). In both cases, an optimal current value with a maximum close to *ca.* 50 at.% Pt is found.

When the electrocatalytic activity of both types of materials is normalized with respect to the total EASA (Fig. 7A), the two curves are close to each other with a difference less than 20%. This suggests that, despite the fact that the structure of the catalysts is radically different in the as-prepared states (mixture of Pt and Au NPs *versus* PtAu alloy NPs), the electrochemical aging process tends to alleviate these differences as a result of the atomic re-arrangement taking place during the CVs in H_2SO_4.

The above consideration does not hold true if the mass activity is used to compare the electrocatalytic activity of the materials for the FAO. For example, the mass activity of $Pt_{45}Au_{55}$ alloy NPs is 0.84 A mg^{-1}, as compared to 0.44 A mg^{-1} for Pt_{44} + Au_{56} mixture NPs. There is a factor of 2 differences between the two materials that would point to a higher activity of PtAu alloy NPs compared to Pt + Au mixture NPs. As discussed previously, it is suspected that the organization of the Pt and Au atoms is such that the surface of the alloys and mixtures resembled closely to each other (compare the CV of Fig. 3D and H) at the end of the electrochemical aging process. So, although some subtle differences might remain between the Pt and Au atomistic organization at the surface of the two types of materials (the CV recorded in the presence of formic acid are not formally identical), it is suspected that another reason is responsible for this difference by a factor of 2. Indeed, it should be remembered that the initial mass of the catalyst is used to compute the mass activities and the residual mass of catalysts left at the electrode surface as a result of the electrochemical aging process might differ from the initial one. Unfortunately, the amount of catalysts left at the surface of the electrode following the electrochemical aging process cannot be easily assessed. And it can be assumed that the dissolution rate of Pt and Au atoms from a mixture of Pt and Au NPs is identical to that of PtAu alloy NPs under potential cycling conditions.

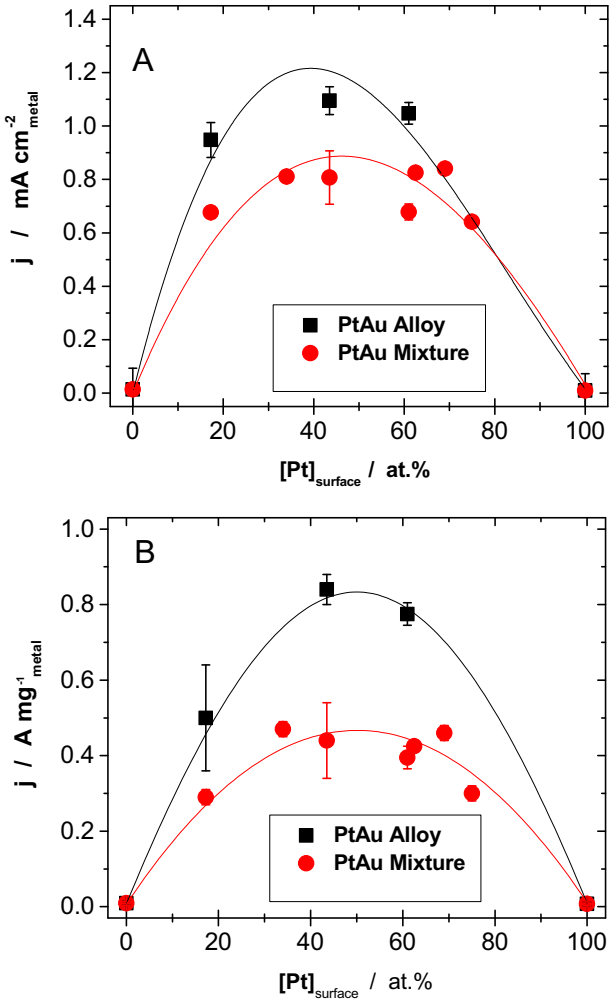

Fig. 7. Potentiostatic current densities (E_{appl} = 0.56 V) in 0.5 M H_2SO_4 + 0.5 M HCOOH as a function of the Pt surface content. The current was read after 600 s of electrolysis. In (A), the current is normalized with respect to the total (Pt + Au) electrochemically active surface area. In (B), the current is expressed in terms with respect to the initial mass of catalysts (A $mg^{-1}{}_{metal}$).

4. Conclusion

Pulsed Laser Ablation in liquid of a single target made of a mixture of Pt and Au powders was used for synthesizing Pt_xAu_{100-x} alloy NPs with a wide range of composition. The mass activity of these alloy NPs for the FAO is maximal for a surface composition close to 50 at.% and reaches *ca* 0.8 A mg^{-1} after 600 s of electrolysis at 0.56 V *vs* RHE. On these alloy NPs, the oxidation of formic acid proceeds mostly according to the direct pathway that involves the dehydrogenation of the molecule. In comparison, as-prepared mixtures of Pt and Au NPs with the same composition exhibit very little activity for the FAO that proceeds through the indirect pathway (dehydration of formic acid). However, a change in the composition and structure of the as-prepared mixtures of Pt and Au NPs occur during an electrochemical aging process that consist in performing CV in 0.5 M H_2SO_4 between 0.05 and an upper potential limit that should not be lower than 1.5 V. It is hypothesized that Pt and Au dissolution and re-deposition occurs during the potential cycling to transforms the catalysts surface so that it adopts a structure close to that of alloy NPs. As a consequence, there is a change of mechanisms and the FAO proceeds also according to the direct pathway. Accordingly, the mass activity of electrochemically

aged mixtures of Pt and Au NPs is only a factor of two lower than that of PtAu alloy NPs. This might be due to a difference in the residual mass of the catalysts owing to different dissolution rates of pure Pt and pure Au NPs on one side, and PtAu alloy NPs, on the other side.

Acknowledgements

This work was supported by the Natural Sciences and Engineering Research Council of Canada (NSERC) through the Strategic Grant Program, the “Fonds de Recherche du Québec: Nature et Technologies (FRQNT) , and the “Agence de l’Efficacité Énergétique du Québec”.

Appendix A. Supplementary data

Supplementary data related to this article can be found at http://dx.doi.org/10.1016/j.jpowsour.2013.09.045.

References

[1] X. Yu, P.G. Pickup, J. Power Sources 182 (2008) 124–132.
[2] Y.W. Rhee, S.Y. Ha, R.I. Masel, J. Power Sources 117 (2003) 35–38.
[3] Y. Zhu, Z. Khan, R.I. Masel, J. Power Sources 139 (2005) 15–20.
[4] J.M. Feliu, E. Herrero, in: W. Vielstich, H.A. Gasteiger, A. Lamm (Eds.), Handbook of Fuel Cells, vol. 2, Wiley, New York, 2003, p. 679.
[5] N.M. Markovic, H.A. Gasteiger, P.N. Ross Jr., X. Jiang, I. Villegas, M.J. Weaver, Electrochim. Acta 40 (1995) 91–98.
[6] S. Ye, in: J. Zhang (Ed.), CO Tolerant Catalysts in PEM Fuel Cell Electrocatalysts and Catalysts Layers, Fundamentals and Applications, Springer-Verlag, 2008, pp. p759–834.
[7] J. Greeley, J.K. Norskov, M. Mavrikakis, Annu. Rev. Phys. Chem. 53 (2002) 319–348.
[8] B. Hammer, J.K. Norskov, Adv. Catal. 45 (2000) 71–129.
[9] A. Ruban, B. Hammer, P. Stoltze, H.L. Skriver, J.K. Norskov, J. Mol. Catal. A: Chem. 115 (1997) 421–429.
[10] W.P. Zhou, A. Lewera, R. Larsen, R.I. Masel, P.S. Bagus, A. Wieckowski, J. Phys. Chem. B 110 (2006) 13393–13398.
[11] N. Hoshi, K. Kida, M. Nakamura, M. Nakada, K. Osada, J. Phys. Chem. B 110 (2006) 12480–12484.
[12] J.H. Choi, K.J. Jeong, Y. Dong, J. Han, T.H. Lim, J.S. Lee, Y.E. Sung, J. Power Sources 163 (2006) 71–75.
[13] J.B. Xu, T.S. Zhao, Z.X. Liang, J. Power Sources 185 (2008) 857–861.
[14] J.K. Lee, J. Lee, J. Han, T.H. Lim, Y.E. Sung, Y. Tak, Electrochim. Acta 53 (2008) 3474–3478.
[15] S. Wang, N. Kristian, S. Jiang, X. Wang, Electrochem. Commun. 10 (2008) 961–964.
[16] Y. Yu, Y. Hu, X. Liu, W. Deng, X. Wang, Electrochim. Acta 54 (2009) 3092–3097.
[17] Z. Peng, H. Yang, Nano Res. 2 (2009) 406–415.
[18] S. Zhang, Y. Shao, G. Yin, Y. Lin, J. Power Sources 195 (2010) 1103–1106.
[19] C. Xu, R. Wang, M. Chen, Y. Zhang, Y. Ding, Phys. Chem. Chem. Phys. 12 (2010) 239–246.
[20] S. Zhang, Y. Shao, G. Yin, Y. Lin, Angew. Chem. Int. Ed. 49 (2010) 2211–2214.
[21] R. Wang, C. Wang, W.B. Cai, Y. Ding, Adv. Mater. 22 (2010) 1845–1848.
[22] C.V. Rao, C.R. Cabrera, Y. Ishikawa, J. Phys. Chem. C 115 (2011) 21963–21970.
[23] S. Zhang, Y. Shao, H.G. Liao, J. Liu, I.A. Aksay, G. Yin, Y. Lin, Chem. Mater. 23 (2011) 1079–1081.
[24] J. Liu, L. Cao, W. Huang, Z. Li, ACS Appl. Mater. Interfaces 3 (2011) 3552–3558.
[25] S. Chen, M. Malig, M. Tian, A. Chen, J. Phys. Chem. C 116 (2012) 3298–3304.
[26] Y. Kim, H.J. Kim, Y.S. Kim, S.M. Choi, M.H. Seo, W.B. Kim, J. Phys. Chem. C 116 (2012) 18093–18100.
[27] I.S. Park, K.S. Lee, J.H. Choi, H.Y. Park, Y.E. Sung, J. Phys. Chem. C 111 (2007) 19126–19133.
[28] D. Pletcher, V. Solis, J. Electroanal. Chem. 131 (1982) 309–323.
[29] J. Clavilier, A. Fernandez-Vega, J.M. Feliu, A. Aldaz, J. Electroanal. Chem. 258 (1989) 89–100.
[30] Y.C. Lu, Z. Xu, H.A. Gasteiger, S. Chen, K. Hamad-Schifferli, Y. Shao-Horn, J. Am. Chem. Soc. 132 (2010) 12170–12171.
[31] Z. Xu, C.E. Carlton, L.F. Allard, Y. Shao-Horn, K. Hamad-Schifferli, J. Phys. Chem. Lett. 1 (2010) 2514–2518.
[32] J. Suntivich, Z. Xu, C.E. Carlton, J. Kim, B. Han, S.W. Lee, N. Bonnet, N. Marzari, L.F. Allard, H.A. Gasteiger, K. Hamad-Schifferli, Y. Shao-Horn, J. Am. Chem. Soc. 135 (2013) 7985–7991.
[33] J. Luo, P.N. Njoki, Y. Lin, D. Mott, L. Wang, C.J. Zhong, Langmuir 22 (2006) 2892–2898.
[34] J. Luo, P.N. Njoki, Y. Lin, L. Wang, C.J. Zhong, Electrochem. Commun. 8 (2006) 581–587.
[35] B.N. Wanjala, J. Luo, R. Loukrakpam, B. Fang, D. Mott, P.N. Njoki, M. Engelhard, H.R. Naslund, J.K. Wu, L. Wang, O. Malis, C.J. Zhong, Chem. Mater. 22 (2010) 4282–4294.
[36] B. Fang, B.N. Wanjala, X. Hu, J. Last, R. Loukrakpam, J. Yin, J. Luo, C.J. Zhong, J. Power Sources 196 (2011) 659.
[37] J. Yin, B. Fang, J. Luo, B. Wanjala, D. Mott, R. Loukrakpam, M.S. Ng, Z. Li, J. Hong, M.S. Whittingham, C.J. Zhong, Nanotechnology 23 (2012) 305404 (8 pp.).
[38] J. Xu, C. Zhang, X. Wang, H. Ji, C. Zhao, Y. Wang, Z. Zhang, Green Chem. 13 (2011) 1914–1922.
[39] Z. Zhang, Y. Wang, X. Wang, Nanoscale 3 (2011) 1663–1674.
[40] J. Zhang, D.N. Oko, S. Garbarino, R. Imbeault, M. Chaker, A. Tavares, D. Guay, D. Ma, J. Phys. Chem. C 116 (2012) 13413–13420.
[41] E. Irissou, F. Laplante, D. Garbarino, M. Chaker, D. Guay, J. Phys. Chem. C 114 (2010) 2192–2199.
[42] S. Xiao, W. Hu, W. Luo, Y. Wu, X. Li, H. Deng, Eur. Phys. J. B 54 (2006) 479–484.
[43] S. Trasatti, O.A. Petrii, Pure Appl. Chem. 63 (1991) 711–734.
[44] D.F. van der Vliet, C. Wang, D. Li, A.P. Paulikas, J. Greeley, R.B. Rankin, D. Strmcnik, D. Tripkovic, N.M. Markovic, V.R. Stamenkovic, Angew. Chem. Int. Ed. 51 (2012) 3139–3142.
[45] S.J. Xia, V.I. Birss, Electrochim. Acta 44 (1998) 467–482.
[46] K.A. Friedrich, F. Henglein, U. Stimming, W. Unkauf, Electrochim. Acta 45 (2000) 3283–3293.
[47] J.P. Hoare, J. Electrochem. Soc. 131 (1984) 1808–1815.
[48] S. Garbarino, A. Pereira, C. Hamel, E. Irissou, M. Chaker, D. Guay, J. Phys. Chem. C 114 (2010) 2980–2988.
[49] E. Pichardo-Pedrero, M. Giesen, Electrochim. Acta 52 (2007) 5659–5668.
[50] M. Giesen, G. Beltramo, S. Dieluweit, J. Müller, H. Ibach, W. Schmickler, Surf. Sci. 595 (2005) 127–137.
[51] S. Cherevko, A.A. Topalov, I. Katsounaros, K.J.J. Mayrhofer, Electrochem. Commun. 28 (2013) 44–46.
[52] C.T. Campbell, S.C. Parker, D.E. Starr, Science 298 (2002) 811–814.
[53] G. Inzelt, B.B. Berkes, A. Kriston, Pure Appl. Chem. 83 (2011) 269–279.
[54] G. Inzelt, B.B. Berkes, A. Kriston, Electrochim. Acta 55 (2010) 4742–4749.
[55] M. Tian, W.G. Pell, B.E. Conway, Corros. Sci. 50 (2008) 2682–2690.
[56] Z. Jusys, S. Bruckenstein, Electrochem. Sol. State Lett. 1 (1998) 74–76.
[57] B.L. Abrams, P.C.K. Vesborg, J.L. Bonde, T.F. Jaramillo, I. Chorkendorff, J. Electrochem. Soc. 156 (2009) B273–B282.
[58] J. Kim, C. Jung, C.K. Rhee, T.H. Lim, Langmuir 23 (2007) 10831–10836.